Ion selectivity of the anthrax toxin channel and its effect on protein translocation

Aviva Schiffmiller,[1] Damon Anderson,[2] and Alan Finkelstein[1]

[1]Department of Physiology and Biophysics, Albert Einstein College of Medicine, Bronx, NY 10461
[2]Acumenta Biotech, Westminster, MA 01473

Anthrax toxin consists of three ∼85-kD proteins: lethal factor (LF), edema factor (EF), and protective antigen (PA). PA_{63} (the 63-kD, C-terminal portion of PA) forms heptameric channels ($(PA_{63})_7$) in planar phospholipid bilayer membranes that enable the translocation of LF and EF across the membrane. These mushroom-shaped channels consist of a globular cap domain and a 14-stranded β-barrel stem domain, with six anionic residues lining the interior of the stem to form rings of negative charges. $(PA_{63})_7$ channels are highly cation selective, and, here, we investigate the effects on both cation selectivity and protein translocation of mutating each of these anionic residues to a serine. We find that although some of these mutations reduce cation selectivity, selectivity alone does not directly predict the rate of protein translocation; local changes in electrostatic forces must be considered as well.

INTRODUCTION

The tripartite anthrax toxin consists of lethal factor (LF; 90 kD), edema factor (EF; 89 kD), and protective antigen (PA; 83 kD). PA forms channels in cell membranes that allow for the passage of LF (a zinc metalloprotease; Duesbery et al., 1998; Vitale et al., 1998) and EF (an adenylate cyclase; Leppla, 1982) into the cytosol, where they interfere with cellular homeostasis and ultimately lead to cell death (for a general review of anthrax toxin, see Young and Collier, 2007). Channel self-assembly begins when monomeric PA binds to either of two known receptors (ANTXR1 and ANTXR2) and is subsequently activated by proteolytic cleavage, which removes the N-terminal 20-kD portion of PA (PA_{20}). The remaining C-terminal 63-kD portion of PA (PA_{63}) then heptamerizes (Young and Collier, 2007) or octamerizes (Kintzer et al., 2009) to form the ring-shaped prepore, which may bind up to three molecules of EF and/or LF. The entire ligand–receptor complex is then endocytosed; in the low pH environment of the endosome, the prepore undergoes conversion to the active $(PA_{63})_7$ pore form. Finally, $(PA_{63})_7$ inserts into the endosomal membrane and facilitates the transfer of EF/LF into the cytosol (Young and Collier, 2007). Although there is no crystal structure of $(PA_{63})_7$, a computer model depicts these channels as mushroom shaped, with a globular cap domain and a cylindrical stem domain (Nguyen, 2004). The ∼100-Å stem is a 14-stranded β-barrel that spans the membrane and extends out of the cell membrane (Benson et al., 1998; Nassi et al., 2002). A recent, high resolution cryo-EM structure of the $(PA_{63})_7$ pore (Fig. 1 B) (Jiang et al., 2015) confirms the structure predicted by the computer model and low resolution EM structures (Katayama et al., 2008; Gogol et al., 2013).

$(PA_{63})_7$ can be reconstituted in planar phospholipid bilayer membranes, forming channels that are capable of translocating LF_N (the N-terminal, 263-residue portion of LF), as well as whole LF and EF, when the appropriate voltage (Zhang et al., 2004b) or pH conditions (Krantz et al., 2006) are applied. Under such conditions, LF_N enters the channel from the cis side (the side to which $(PA_{63})_7$ has been added), N terminus first (Zhang et al., 2004a), passes through the channel cap and stem, and then exits into the trans solution (Finkelstein, 2009). In the absence of translocating protein, these channels have a conductance of ∼55 pS (in 100 mM KCl, pH 5.5) (Krantz et al., 2005) and are highly (although not ideally) selective for cations (Blaustein and Finkelstein, 1990). The mechanistic basis behind both pH- and voltage-driven translocation through the $(PA_{63})_7$ channel is critically dependent on the channel's cation selectivity. At pH 5.5, LF_N bears a net negative charge of −6. Because LF_N translocation through the channel occurs when positive voltages are applied to the cis solution, the carboxyl groups on LF_N must be neutralized for voltage-driven translocation to occur. However, at pH 5.5, the carboxyl groups on aspartate and glutamate residues are in the ionized form ∼97% of the time. Nonetheless, it is the minority protonated form that is favored for entry into the channel, largely because of the cation

Correspondence to Aviva Schiffmiller: avivaschiffmiller@gmail.com

Abbreviations used in this paper: EF, edema factor; GHK, Goldman–Hodgkin–Katz; LF, lethal factor; MTS-ES, 2-sulfonatoethyl MTS; PA, protective antigen.

The Rockefeller University Press $30.00
J. Gen. Physiol. Vol. 146 No. 2 183–192
www.jgp.org/cgi/doi/10.1085/jgp.201511388

selectivity of the channel (Finkelstein, 2009). Similarly, a pH gradient in which the pH of the cis solution is lower than that of the trans solution will also cause LF_N translocation to occur, as the aspartate and glutamate residues on LF_N are more likely to exist in their protonated form on the cis side than on the trans side. Therefore, the rate of entry of these residues into the channel is greater from the cis side than from the trans side because of the cation selectivity of the channel, biasing the Brownian motion of LF_N toward the trans side (Krantz et al., 2006).

Each of the seven monomers of $(PA_{63})_7$ contributes a phenylalanine residue, F427, to form a ring known as the phenylalanine clamp (Φ-clamp), located at the junction between the cap and stem domains of the channel. The Φ-clamp creates a tight seal around the translocating peptide, facilitating the unfolding of the protein as well as creating a near-complete block in ion conductance that is important for efficient translocation (Krantz et al., 2005). It has also been identified as an important site of anion exclusion (Basilio et al., 2009): adding a single nontitratable sulfonate group at most positions on LF_N largely abolishes translocation, as the channel strongly disfavors the entry of negatively charged groups, but mutating the residues of the Φ-clamp to alanine residues ($(PA_{63}F427A)_7$) restores translocation (Basilio et al., 2009). These results are consistent with the observation that mutating the Φ-clamp residues to alanine residues reduces the K^+/Cl^- selectivity of the channel (Basilio et al., 2009).

In addition to the Φ-clamp residues, it is also expected that the six rings of negatively charged residues that line the channel stem (D276, E302, E308, D315, D335, and E343; see Fig. 1 A) may contribute to the cation selectivity of the channel. In this paper, we explore the effect on both cation selectivity and protein translocation when each of these anionic residues is mutated to a serine residue. Although we find that specific anionic mutations may reduce macroscopic selectivity and/or impede translocation, the local distribution of the anionic residues in the channel must be considered as well.

MATERIALS AND METHODS

Molecular biology and protein purification

The pET-22b (EMD Millipore) vectors encoding PA_{83}D276S, PA_{83}E302S, PA_{83}E308S, PA_{83}D315S, PA_{83}D335S, PA_{83}E343S, and PA_{83}E302S/E308S/D315S were constructed using a pET-22b vector encoding WT PA_{83} (provided by J. Collier, Harvard Medical School, Boston, MA) and the QuikChange Site-Directed Mutagenesis kit (Agilent Technologies). PA_{83}D276S, PA_{83}E308S, PA_{83}D315S, and PA_{83}D335S were recombinantly expressed, purified, and nicked with trypsin (to detach PA_{20} and leave behind PA_{63}) as described previously (Benson et al., 1998). PA_{83}E302S, PA_{83}E343S, and PA_{83}E302S/E308S/D315S were expressed, purified, and then nicked with trypsin according to a slightly different protocol as described previously (Anderson and Blaustein, 2008).

WT $(PA_{63})_7$ (trypsin-treated PA_{83} from which PA_{20} was detached; Blaustein et al., 1989) was provided by S. Zhang (Harvard Medical School, Boston, MA). $(PA_{63}F427A)_7$ was the same sample reported previously (Krantz et al., 2005). LF_N (the N-terminal, 263 residues of LF, containing the EMD Millipore His_6-tag at the N terminus) and LF_N A59C 2-sulfonatoethyl MTS (MTS-ES; LF_N with an N-terminal His_6-tag and a sulfonate group attached at residue 59, which has been mutated to a cysteine) were also the same samples reported previously (Basilio et al., 2009). The His_6-tags on LF_N and LF_N A59C MTS-ES were cleaved with thrombin according to EMD Millipore's instructions.

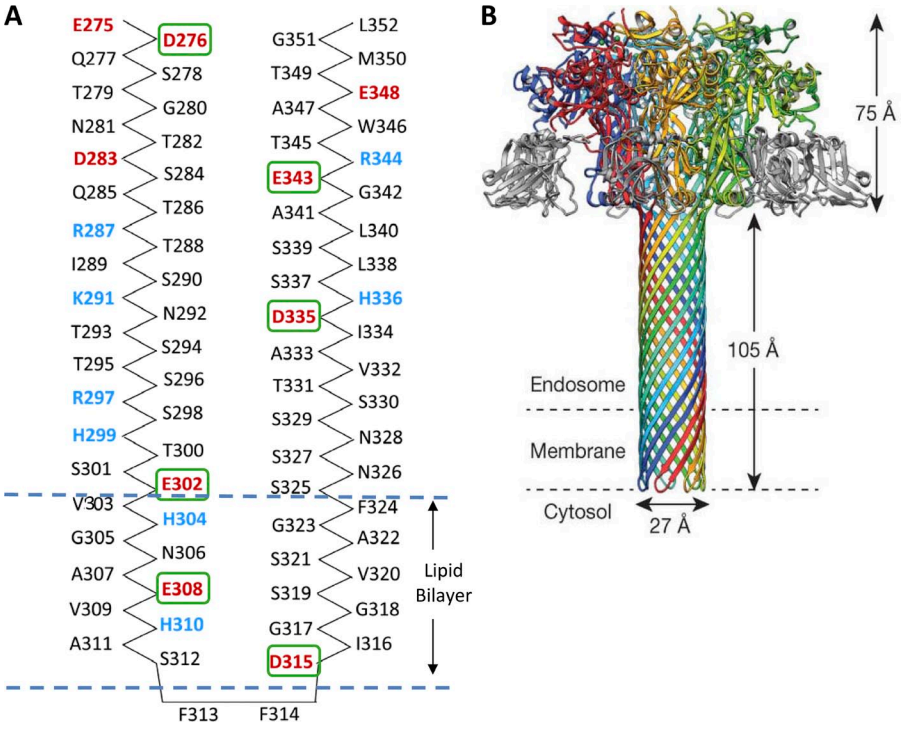

Figure 1. (A) Residues that line the channel lumen and exterior of the $(PA_{63})_7$ stem. Anionic residues are highlighted in red; cationic residues are highlighted in blue. The six anionic residues lining the lumen are circled in green. Horizontal dashed blue lines represent the lipid bilayer (adapted from Nassi et al., 2002). (B) Cryo-EM structure (Jiang et al., 2015) of the $(PA_{63})_7$ channel (resolution of 2.9 Å). Horizontal dashed lines represent the lipid bilayer.

Planar lipid bilayers

Planar lipid bilayers were formed using the brush technique (Mueller et al., 1963) across a 0.5-mm hole in a Teflon partition. The partition divided a Lucite chamber into two compartments that each held 3 ml of 250 mM KCl (or 100 mM KCl), 5 mM potassium-succinate, and 1 mM EDTA, pH 5.5; each compartment was stirred using tiny magnetic stir bars. Agar salt bridges (3 M KCl; 3% agar) connected Ag/AgCl electrodes in saturated KCl solutions to the two compartments. The lipid solution was 3% diphytanoyl-phosphatidylcholine (Avanti Polar Lipids, Inc.) in *n*-decane. Membrane formation was observed visually. Experiments were all performed under voltage-clamp conditions; voltages are taken as those of the cis solution with respect to the trans solution (held at virtual ground). Current responses were filtered at 1 Hz by a low-pass eight-pole Bessel filter (Warner Instruments), recorded on a DMP-4B Physiograph chart recorder (Narco Bio Systems), and digitally stored using NI USB-6211 Data Acquisition Board (National Instruments) (Basilio et al., 2009; Schiffmiller and Finkelstein, 2015).

Selectivity profiles

After a lipid bilayer was formed, $(PA_{63})_7$ prepore heptamer (or one of the mutant prepore heptamers) was added to the cis solution (250 or 100 mM KCl, 5 mM potassium-succinate, and 1 mM EDTA, pH 5.5), causing the formation of hundreds to thousands of channels in the lipid bilayer. 3 M KCl was then added in incremental amounts to the cis solution (an incremental amount of solution was withdrawn before each 3-M KCl incremental addition), and for each increment, the reversal potential (E_{rev}) was recorded. Reversal potentials were plotted against KCl activity ratios (a_{cis}/a_{trans}) using activity coefficients recorded in the literature (Robinson and Stokes, 1965). The K^+ concentration was taken as equal to the KCl concentration; it was estimated that 10 mM K^+ was contributed by potassium-succinate and potassium-EDTA.

Translocation experiments

After a lipid bilayer was formed, $(PA_{63})_7$ prepore heptamer (or one of the mutant prepore heptamers) was added to the cis solution (250 mM KCl, 5 mM potassium-succinate, and 1 mM EDTA, pH 5.5). Once conductance leveled off at 20 mV, LF_N (or LF_N A59C MTS-ES) was added to the cis compartment to a final concentration of ~3 nM. Excess ligand was subsequently removed by perfusing the cis solution; the exchange of five volumes was performed using a manual pump while the voltage was held at 20 mV. The voltage was then switched to 3 mV, and a small amount of 1 M potassium phosphate (dibasic) was added to the trans solution to raise the pH to either 6.15 or 6.5. After 15 s, the voltage was switched back to 20 mV to allow translocation to take place. To determine the rate of translocation, we normalized the final conductance to the conductance observed at 20 mV after the channels were unblocked at −50 or −55 mV for 30 s (Basilio et al., 2009).

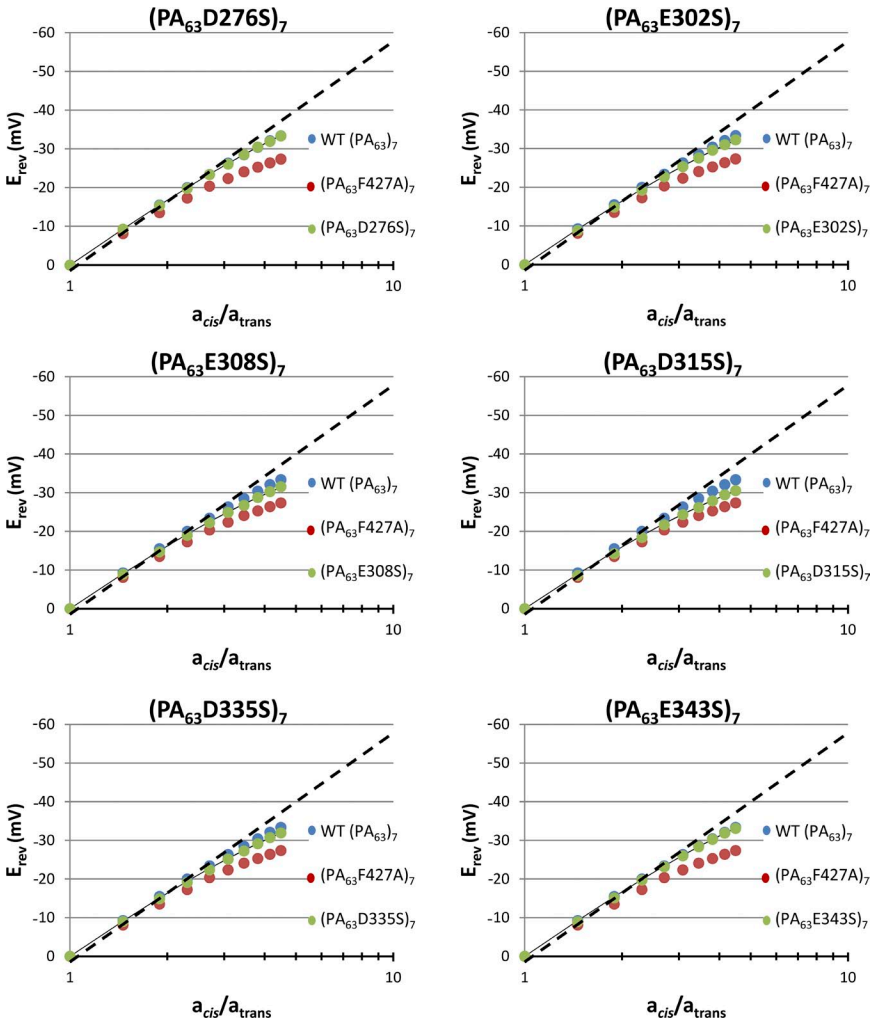

Figure 2. Plots of E_{rev} versus activity ratios of KCl (a_{cis}/a_{trans}) (on a logarithmic scale) of asp/glu mutant channels with $[KCl]_{trans}$ = 100 mM KCl. For comparison, plots of WT and $(PA_{63}F427A)_7$ channels are also shown. Dashed black lines represent ideal cation selectivity. All experiments were performed in triplicate. In some instances, the WT data points are obscured by the asp/glu mutant channel data points because their selectivity is nearly identical. Error bars represent standard deviation for the asp/glu mutant channels; bars that are not visible are so small that they are obscured by the symbol. The curves connecting the asp/glu mutant channel data points are the best fit of Eq. 1 to these points, where [N] is the value given for each asp/glu mutant channel at 100 mM KCl in Table 2.

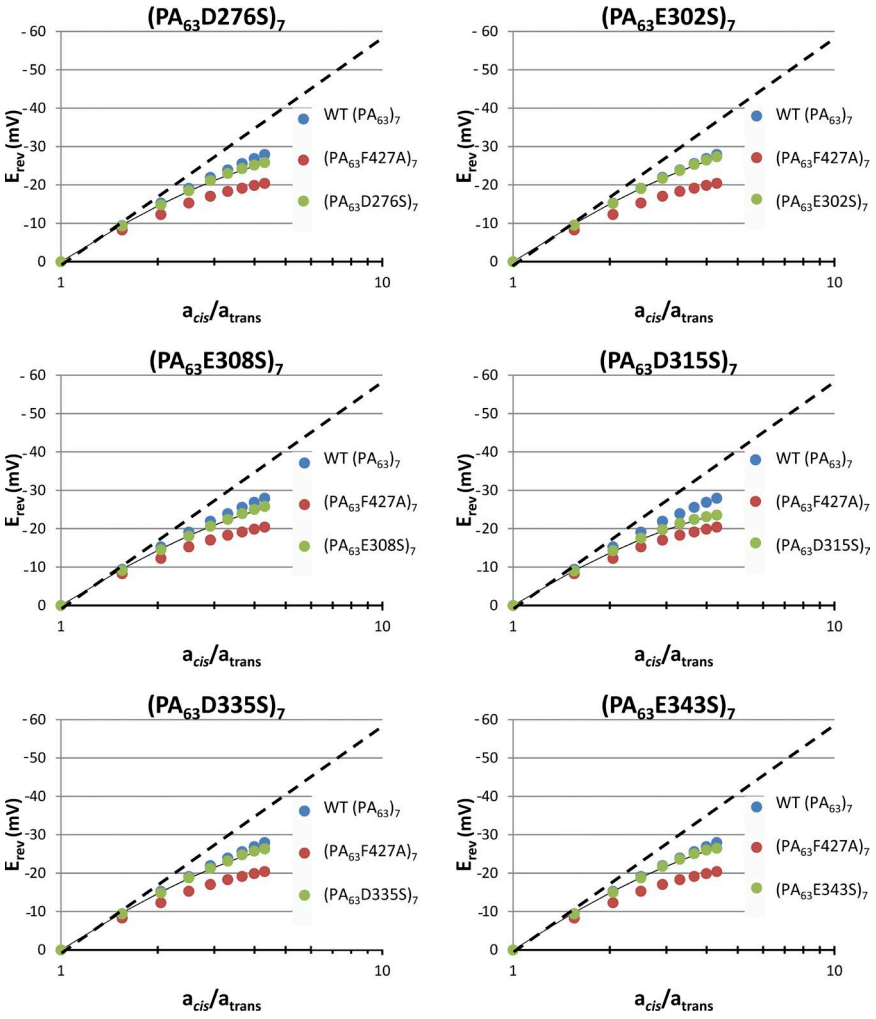

Figure 3. Plots of E_{rev} versus activity ratios of KCl (a_{cis}/a_{trans}) (on a logarithmic scale) of asp/glu mutant channels with $[KCl]_{trans}$ = 250 mM KCl. For comparison, plots of WT and $(PA_{63}F427A)_7$ channels are also shown. Dashed black lines represent ideal cation selectivity. All experiments were performed in triplicate. In some instances, the WT data points are obscured by the asp/glu mutant channel data points because their selectivity is nearly identical. Error bars represent standard deviation for the asp/glu mutant channels; bars that are not visible are so small that they are obscured by the symbol. The curves connecting the asp/glu mutant channel data points are the best fit of Eq. 1 to these points, where [N] is the value given for each asp/glu mutant channel at 250 mM KCl in Table 2.

Online supplemental material

Fig. S1 shows that the plots of E_{rev} versus the ratio of KCl activities are adequately fit at both $[KCl]_{trans}$ = 100 mM and $[KCl]_{trans}$ = 250 mM by the same [N] for a given channel. Fig. S2 shows that the single-channel conductance of WT $(PA_{63})_7$ channels is comparable to that of the $(PA_{63}E302S/E308S/D315S)_7$ channels (100 pS vs. 80–90 pS, respectively) in 250 mM KCl at 20 mV. Fig. S3 shows records of the single-channel conductance of both the $(PA63E302S/E308S/D315S)_7$ channel as well as the WT $(PA63)_7$ channel. The online supplemental material is available at http://www.jgp.org/cgi/content/full/jgp.201511388/DC1.

RESULTS

Ion selectivity profiles of the asp/glu mutant channels

We generated ion selectivity profiles for each of the six asp/glu mutant channels: $(PA_{63}D276S)_7$, $(PA_{63}E302S)_7$, $(PA_{63}E308S)_7$, $(PA_{63}D315S)_7$, $(PA_{63}D335S)_7$, and $(PA_{63}E343S)_7$. After inserting channels of a given type into a membrane separating symmetric solutions of 100 mM KCl, pH 5.5, we raised the KCl concentration of the cis compartment by adding incremental amounts of concentrated KCl; for each increment, we recorded the reversal potential (E_{rev}). We then plotted E_{rev} versus the activity ratio (a_{cis}/a_{trans}) of KCl (Fig. 2) and compared these profiles to those of WT $(PA_{63})_7$ and $(PA_{63}F427A)_7$ channels. We also repeated these experiments beginning with symmetric solutions of 250 mM KCl, pH 5.5 (Fig. 3).

Applying the Goldman–Hodgkin–Katz (GHK) equation (Hodgkin and Katz, 1949), we were able to roughly calculate the permeability ratio (P_K/P_{Cl}) for each

TABLE 1
Permeability ratios (P_K/P_{Cl}) of channels

Channel	100 mM KCl	250 mM KCl
WT $(PA_{63})_7$	22.2	9.1
$(PA_{63}E302S)_7$	17.5	8.9
$(PA_{63}E343S)_7$	20.8	8.7
$(PA_{63}D276S)_7$	20.8	8.3
$(PA_{63}D335S)_7$	15.4	8.2
$(PA_{63}E308S)_7$	14.7	7.7
$(PA_{63}D315S)_7$	12.2	6.5
$(PA_{63}F427A)_7$	9.5	4.6

Permeability ratios (P_K/P_{Cl}) of channels, calculated by applying the GHK equation to the cation selectivity profiles of each channel with $[KCl]_{trans}$ = 100 and 250 mM KCl. Numbers represent P_K/P_{Cl}.

TABLE 2

Negative fixed charge density (molarity) of channels

Channel	100 mM KCl	250 mM KCl	Mean
WT $(PA_{63})_7$	0.70	0.85	0.78
$(PA_{63}E302S)_7$	0.60	0.83	0.72
$(PA_{63}E343S)_7$	0.68	0.80	0.74
$(PA_{63}D276S)_7$	0.70	0.74	0.72
$(PA_{63}D335S)_7$	0.58	0.77	0.68
$(PA_{63}E308S)_7$	0.55	0.72	0.64
$(PA_{63}D315S)_7$	0.50	0.63	0.57
$(PA_{63}F427A)_7$	0.38	0.48	0.43

Negative fixed charge density (molarity) of channels (calculated from Eq. 1) with $[KCl]_{trans}$ = 100 and 250 mM KCl. Each entry is the value of [N] that fits the data in Figs. 2 and 3.

mutant channel (Table 1). As expected (Basilio et al., 2009), the value of P_K/P_{Cl} for the $(PA_{63}F427A)_7$ channel was significantly smaller than that for the WT $(PA_{63})_7$ channel at both salt concentrations by a factor of ~2. In terms of the asp/glu mutant channels, at both salt concentrations, the $(PA_{63}D315S)_7$ channel was the least cation selective (although not as poor as that of $(PA_{63}F427A)_7$), followed by $(PA_{63}E308S)_7$. At 250 mM KCl, the other asp/glu mutant channels did not have cation selectivities that were very different from that of the WT channel, whereas at 100 mM KCl, the $(PA_{63}D335S)_7$ and $(PA_{63}E302S)_7$ channels were somewhat less cation selective than the WT $(PA_{63})_7$ channel.

An interesting aspect of the preceding data is that for each channel type, the reversal potential for a given KCl activity ratio is smaller if the ratio is taken with respect to 250 mM KCl rather than to 100 mM KCl (Figs. 2 and 3). In terms of the GHK permeability coefficients, this is expressed by the fact that P_K/P_{Cl} is smaller (Table 1). This phenomenon arises naturally if the basis for the cation selectivity of the channel is that it bears a net negative charge. In a simplistic model of the channel in which we assume that it is a fixed charge membrane of uniform fixed charge density, then the reversal potential E_{rev} across the membrane is given by the algebraic sum of the Donnan potentials at the two membrane–solution interfaces (Teorell, 1953):

$$E_{rev} = \frac{RT}{F} \ln \frac{r_{cis}}{r_{trans}},$$

where

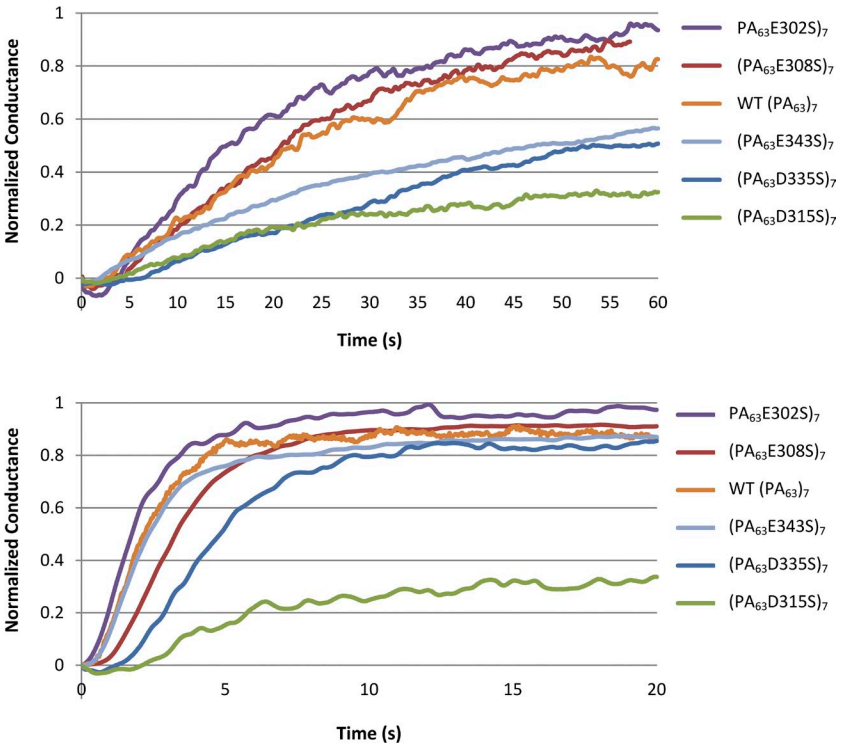

Figure 4. The effect of mutating the anionic residues in the anthrax toxin channel stem on the rate of pH-driven LF_N translocation (top, ΔpH = 0.65; bottom, ΔpH = 1.0). Each graph shows the normalized (see Materials and methods) increase in conductance that occurs (after perfusion of excess LF_N out of the cis compartment) upon raising the pH of the trans compartment from pH 5.5 to pH 6.15 (top) or pH 6.5 (bottom) by adding a small amount of potassium phosphate (1 M, dibasic). Note the difference in the timescale between the two graphs; as is expected, translocation occurs at a much faster rate at ΔpH = 1.0. Experiments were performed in 250 mM KCl.

TABLE 3

Halftimes ($t_{1/2}$, in seconds) of LF_N translocation at ΔpH = 0.65 and 1.0

Channel	$t_{1/2}$, ΔpH = 0.65	$t_{1/2}$, ΔpH = 1
WT $(PA_{63})_7$	23 ± 0.26	2.7 ± 0.55
$(PA_{63}E302S)_7$	20 ± 4.4	2.1 ± 0.49
$(PA_{63}E308S)_7$	22 ± 2.5	4.0 ± 0.83
$(PA_{63}D315S)_7$	n/a	n/a
$(PA_{63}D335S)_7$	50 ± 7.2	4.9 ± 0.96
$(PA_{63}E343S)_7$	43 ± 6.0	2.5 ± 0.42

Halftimes ($t_{1/2}$, in seconds) of LF_N translocation at ΔpH = 0.65 and 1.0. Each halftime represents the mean $t_{1/2}$ of three experiments. Note that for the $(PA_{63}D315S)_7$ channel, translocation was too slow to observe $t_{1/2}$. n/a, not applicable.

$$\frac{r_{cis}}{r_{trans}} = \frac{\frac{z[N]}{2c_{trans}} + \sqrt{\left(\frac{z[N]}{2c_{trans}}\right)^2 + 1}}{\frac{z[N]}{2c_{cis}} + \sqrt{\left(\frac{z[N]}{2c_{cis}}\right)^2 + 1}}, \quad (1)$$

and R is the gas constant, T is temperature in degrees Kelvin, F is the Faraday constant, r is the Donnan ratio, N is the concentration of fixed negative charges, c is ion activity, and z is the charge, which in our case is −1. (Because the mobilities of K^+ and Cl^- are approximately equal, the diffusion potential within the membrane is approximately zero and hence does not contribute to E_{rev}.) The negative fixed charge concentration calculated for each channel is shown in Table 2; we obtained comparable values of [N] at both 100 and 250 mM KCl.

We see in Fig. S1 that for each channel type, the plots of E_{rev} versus the ratio of KCl activities are adequately fit at both $[KCl]_{trans}$ = 100 mM and $[KCl]_{trans}$ = 250 mM by the same [N]. The advantages of this approach compared with the GHK equation will be addressed in the Discussion.

pH-driven LF_N translocation through the asp/glu mutant channels

Although we wished to observe the effects of mutating the anionic residues in the anthrax toxin stem on both voltage- and pH-driven translocation, we unfortunately encountered significant voltage-dependent gating at high positive voltages (e.g., 50 mV) in several of the asp/glu mutant channels ($(PA_{63}E308S)_7$, $(PA_{63}D315S)_7$, and $(PA_{63}D335S)_7$), thereby making it very difficult to interpret the kinetics of LF_N translocation. Consequently, we were limited to the study of pH-driven translocation. All experiments were performed in 250 mM KCl to minimize gating that occurred at even small positive voltages (e.g., 20 mV).

At ΔpH = 0.65 (Fig. 4, top, and Table 3), the rate of LF_N translocation through $(PA_{63}E302S)_7$ and $(PA_{63}E308S)_7$ channels (halftimes [$t_{1/2}$]: 20 and 22 s, respectively) was basically the same as that for the WT channel ($t_{1/2}$: 23 s). On the other hand, $(PA_{63}D335S)_7$ and $(PA_{63}E343S)_7$ channels exhibited significantly slower translocation rates ($t_{1/2}$: 50 and 43 s, respectively), and the $(PA_{63}D315S)_7$ channel exhibited the slowest translocation rate of all (the halftime was too slow to be measured).

At ΔpH = 1.0 (Fig. 4, bottom, and Table 3), where LF_N translocation occurs on a much faster timescale, the $(PA_{63}D315S)_7$ channel still exhibited slow translocation (once again, the halftime was too slow to be measured). Meanwhile, all of the other asp/glu mutant channels

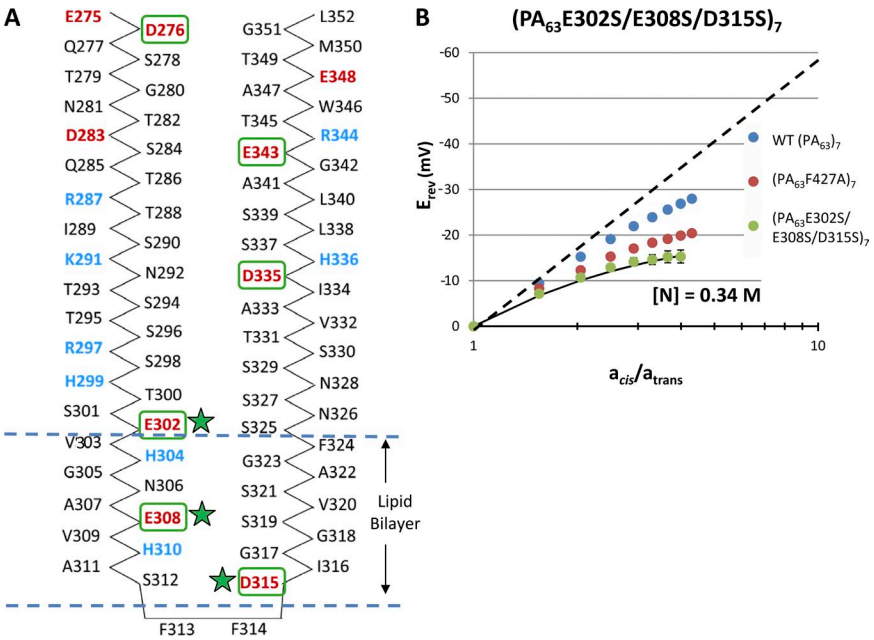

Figure 5. (A) Residues that line the interior and exterior of the $(PA_{63})_7$ stem. Anionic residues are highlighted in red; cationic residues are highlighted in blue. The six anionic residues lining the interior interface are circled in green. Horizontal dashed blue lines represent the lipid bilayer. Green stars indicate the anionic residues that were mutated to serines to generate $(PA_{63}E302S/E308S/D315S)_7$ (adapted from Nassi et al., 2002). (B) Ion selectivity profile of the triple asp/glu mutant channel, $(PA_{63}E302S/E308S/D315S)_7$, compared with that of the WT and $(PA_{63}F427A)_7$ channels, performed in 250 mM KCl. The dashed black line represents ideal cation selectivity. All experiments were performed in triplicate. Error bars represent standard deviation for the $(PA_{63}E302S/E308S/D315S)_7$ channel; bars that are not visible are so small that they are obscured by the symbol. The curve connecting the $(PA_{63}E302S/E308S/D315S)_7$ channel data points is the best fit of Eq. 1 to these points, where [N] = 0.34 M.

exhibited very similar translocation rates to that of the WT channel ($t_{1/2}$: 2.5 s), except for $(PA_{63}D335S)_7$ ($t_{1/2}$: 4.9 s) and the $(PA_{63}E308S)_7$ channel ($t_{1/2}$: 4.0 s).

Unfortunately, we were not able to observe translocation for the $(PA_{63}D276S)_7$ channel, because LF_N exhibited poor binding to this channel at this salt concentration (250 mM KCl). Because residue D276 is located near the top of the stem, we suspect that it may play a role in "clamping" LF_N and holding the peptide in place when it first enters the channel. Also, we were unable to perform pH-driven translocation experiments with the $(PA_{63}F427A)_7$ channel, as it has been demonstrated that mutating the Φ-clamp to alanine residues abolishes pH-driven translocation (likely by collapsing the proton gradient across the Φ-clamp) (Krantz et al., 2005).

What is clear from these results is that the ion selectivity of a given mutant channel is not a direct predictor of the rate of translocation. It is true that $(PA_{63}D315S)_7$, which exhibits the poorest cation selectivity of all the mutant channels (Table 1), has significantly slower translocation rates than those of the WT channel at both pH gradients (Fig. 4). However, although the $(PA_{63}E308S)_7$ channel is also noticeably less cation selective than WT $(PA_{63})_7$, the E308S mutation does not seem to impede pH-driven translocation at ΔpH = 0.65 (Fig. 4, top). Conversely, $(PA_{63}E343S)_7$ is nearly as cation selective as the WT channel (Table 1), yet it exhibits slower LF_N translocation at ΔpH = 0.65 (Fig. 4, top).

pH-driven translocation of LF_N with a sulfonate group attached

As mentioned above, the Φ-clamp has been identified as a site of anion exclusion during protein translocation through the anthrax toxin channel, and mutating the phenylalanine residues of the Φ-clamp to alanines allows for the passage of a nontitratable sulfonate group ($-SO_3^-$) attached to LF_N (Basilio et al., 2009). We wished to determine whether a sulfonate group is able to pass through an asp/glu mutant channel that has an intact Φ-clamp but very poor cation selectivity. For this experiment, we chose a triple mutant channel, $(PA_{63}E302S/E308S/D315S)_7$, whose cation selectivity is even poorer than that of $(PA_{63}F427A)_7$ (Fig. 5 B). As an aside, preliminary data have shown that the channels formed by the triple mutant channel have a single-channel conductance that is slightly smaller than that of the WT channel, but tend to open and close more frequently than does the WT channel (Fig. S2).

We observed pH-driven translocation of LF_N A59C MTS-ES (LF_N in which residue 59 is mutated from an alanine to a cysteine, followed by incubation with MTS-ES to attach a sulfonate group; Basilio et al., 2009) in both WT $(PA_{63})_7$ and $(PA_{63}E302S/E308S/D315S)_7$ channels at a ΔpH of 1 (Fig. 6). As a control, we also observed the translocation of WT LF_N through both channels. Whereas the translocation of LF_N A59C MTS-ES through the WT channel was mostly abolished, there was virtually no translocation at all through the $(PA_{63}E302S/E308S/D315S)_7$ channel either. Thus, despite the poor cation selectivity of the triple mutant channel, it does not allow the passage of SO_3^-. It should be emphasized that this effect was not caused by steric hindrance of the bulky sulfonate group, as the similarly sized trimethylammonium group ($-N(CH_3)_3^+$), attached to LF_N at the same location as the sulfonate group (residue 59), was able to pass through the triple mutant channel unhindered (unpublished data).

DISCUSSION

Ion selectivity

In this paper, we observed the effects of mutating each of the six anionic residues lining the interior of the anthrax toxin channel to serines. Before discussing the effects of these mutations on cation selectivity, we must first address the possibility that streaming potentials and/or polarization effects (dilution potentials) may have skewed our results. By polarization effects, we mean that as a consequence of osmotic water flow across the membrane from the trans to the cis solution caused by the higher KCl concentration in the cis compartment, the KCl concentration at the cis membrane–solution interface is reduced, and at the trans membrane–solution interface it is elevated. Consequently, the actual a_{cis}/a_{trans}

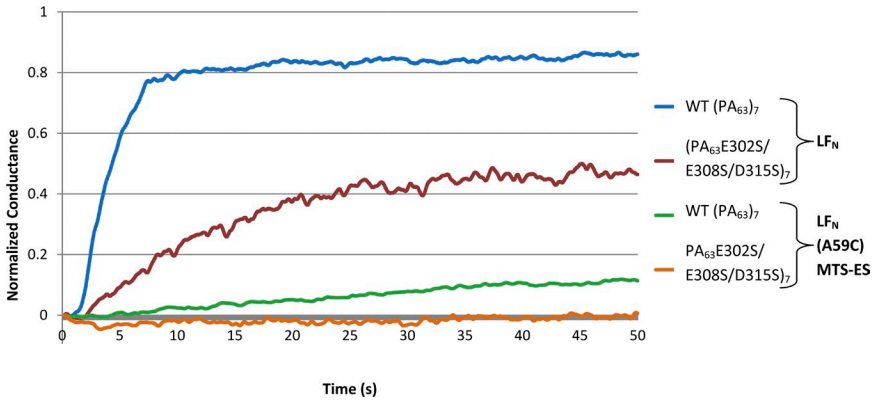

Figure 6. The effect of introducing an SO_3^- group in LF_N on the rate of pH-driven LF_N translocation in WT $(PA_{63})_7$ and $(PA_{63}E302S/E308S/D315S)_7$ channels. Residue 59 of LF_N was mutated from an alanine to a cysteine, followed by incubation of LF_N A59C with MTS-ES to attach a sulfonate group (Basilio et al., 2009). The graph shows the normalized increase in conductance that occurs (after perfusion of excess LF_N out of the cis compartment) upon raising the pH of the trans compartment from pH 5.5 to pH 6.5 by adding a small amount of potassium phosphate (1 M, dibasic). Experiments were performed in 250 mM KCl.

across the membrane is less than the bulk a_{cis}/a_{trans}, thereby artificially reducing the magnitude of E_{rev}. To check for polarization effects, we performed cation selectivity experiments (not depicted) with valinomycin (which is ideally selective for potassium) at both $[KCl]_{trans}$ = 100 mM and $[KCl]_{trans}$ = 250 mM. At both salt concentrations, the reversal potential profiles for valinomycin (at the same a_{cis}/a_{trans} as in the $(PA_{63})_7$ experiments) did not deviate from ideal selectivity, indicating that no polarization is taking place.

As far as streaming potentials are concerned, note that if streaming potentials were an issue, the greatest "bending" of the selectivity profiles should be observed with the WT channel, as it is more cation selective than any of the mutant channels (Tables 1 and 2). On the contrary, the reverse is the case (Figs. 2 and 3). Furthermore, any bending of the selectivity profiles of the mutant channels caused by streaming potentials is expected to be even less significant, as the mutant channels are less cation selective than the WT channel (Tables 1 and 2). Thus, we believe that the cation selectivity profiles that we have generated for the mutant channels have not been significantly affected by streaming potentials.

Using the GHK equation, we calculated the permeability ratio (P_K/P_{Cl}) for the WT channel, the $(PA_{63}F427A)_7$ mutant channel, and the six asp/glu mutant channels (Table 1) at both $[KCl]_{trans}$ = 100 mM and $[KCl]_{trans}$ = 250 mM. To reiterate our findings, P_K/P_{Cl} was much smaller for the $(PA_{63}F427A)_7$ channel than for the WT $(PA_{63})_7$ channel at both salt concentrations, whereas the $(PA_{63}D315S)_7$ channel exhibited the next poorest cation selectivity, followed by $(PA_{63}E308S)_7$. At 250 mM $[KCl]_{trans}$, the other asp/glu mutant channels had similar cation selectivities to that of the WT channel, whereas at 100 mM $[KCl]_{trans}$, the $(PA_{63}D335S)_7$ and $(PA_{63}E302S)_7$ channels were a little less selective than the WT $(PA_{63})_7$ channel.

Although widely used, the GHK equation has certain deficiencies. The particular one that concerns us here is that it assumes that the partition coefficients of K^+ and Cl^- between the solution and the channel are constant, independent of salt concentration. In practice, we see that the permeability ratios calculated at $[KCl]_{trans}$ = 250 mM are much smaller than those calculated at $[KCl]_{trans}$ = 100 mM (Table 1), whereas the GHK equation implies, at face value, that the permeability ratio is independent of salt concentration.

A simple explanation for the difference in cation selectivity at the two salt concentrations ($[KCl]_{trans}$ = 100 mM and 250 mM) is the existence of fixed negative charges in the channels. For this reason, we simplistically modeled the channels as a membrane with a uniform fixed negative charge density, using Eq. 1 (Teorell, 1953). Although this is a gross oversimplification of the distribution of negative charges in the $(PA_{63})_7$ channels, it has the advantage that the poorer cation selectivity we observe when $[KCl]_{trans}$ = 250 mM arises as a natural consequence of the model (see Eq. 1). We see, in fact, that a given [N] adequately fits the selectivity data for both 100 and 250 mM KCl for each channel type (Fig. S1). We emphasize that this model cannot be taken literally: if the distribution of negative fixed charge density in the channel was indeed uniform, then selectivity should be affected in the same manner regardless of which asp/glu residue was mutated. Furthermore, the $(PA_{63}F427A)_7$ channel exhibited worse cation selectivity (P_K/P_{Cl}) than the WT channel by a factor of ~2 (Table 1) and was thus modeled as having a smaller value of [N], yet no actual charges were mutated in the Φ-clamp mutant channel.

Translocation

Our results of pH-driven translocation of LF_N through the WT $(PA_{63})_7$ channel, as well as through five of the six asp/glu mutant channels (Fig. 4 and Table 3), indicate that the translocation rates through these channels are not necessarily correlated with cation selectivity. At ΔpH = 0.65 (in 250 mM KCl), the $(PA_{63}D315S)_7$, $(PA_{63}D335S)_7$, and $(PA_{63}E343S)_7$ channels all exhibited significantly slower translocation rates than through the WT channel (Fig. 4, top, and Table 3). That the translocation rate through the $(PA_{63}D315S)_7$ channel was the slowest is consistent with its being the least anion exclusionary of the six asp/glu mutant channels at this salt concentration (Table 1). However, it is not obvious why the $(PA_{63}D335S)_7$ and $(PA_{63}E343S)_7$ channels should have such slow translocation rates, given that the cation selectivities of these two channels are comparable to that of the WT channel (Table 1).

This observation emphasizes that to truly understand translocation through the anthrax toxin channel, we must consider not only macroscopic cation selectivity but rather the local electrostatic forces acting in the channel as well. A previous electrostatic modeling study (Wynia-Smith et al., 2012) has suggested that there exist two areas of opposite charge in the channel stem, comprised of an anion-repulsive region (the top of the stem) and a cation-repulsive region (the middle of the stem). These electrostatic forces are generated by the charged residues lining both the lumen and exterior of the channel stem (Fig. 1 A). D276, D335, and E343 have been identified as residues that contribute to the anion-repulsive region (Wynia-Smith et al., 2012) and may be part of an "ion selectivity filter" that includes the Φ-clamp. The model that has been proposed is that once the appropriate pH gradient has been established, a polypeptide substrate can pass through the anion-repulsive feature of the upper stem after its aspartate and glutamate residues are protonated by the low pH of the cis solution (Wynia-Smith et al., 2012). As the polypeptide moves farther down the channel, the higher pH of the trans solution will deprotonate its aspartate and glutamate residues, propelling it away from the anion-repulsive region.

The cation-repulsive region will also favor deprotonation of these residues. In this way, an electrostatic "ratchet" is imposed on the substrate, biasing its movement toward the trans solution and preventing reverse translocation of the chain.

Thus, if D335 and E343 are indeed important components of this electrostatic ratchet, then it is understandable that at ΔpH = 0.65, mutating these residues to serines would result in slow, inefficient translocation compared with what is observed in the WT channel (Fig. 4, top). On the other hand, at ΔpH = 1.0, LF_N translocation in the $(PA_{63}E343S)_7$ channel is comparable to that of the WT channel, whereas translocation in the $(PA_{63}D335S)_7$ channel is only a little slower (Fig. 4, bottom). Perhaps the larger pH gradient results in more efficient deprotonation of the polypeptide chain once it moves down the channel stem (closer to the trans solution), compensating for any interference of the D335S/E343S mutations with the electrostatic ratchet.

Finally, we also sought to identify the defining feature that prevents a nontitratable sulfonate group ($-SO_3^-$) from passing through the $(PA_{63})_7$ channel. Although mutating the Φ-clamp residues to alanines allows for the translocation of a sulfonate group attached at most locations on LF_N (Basilio et al., 2009), it was simply not clear at the time whether this phenomenon was caused by reducing the macroscopic cation selectivity of the channel or by possible changes in the local electric field, caused by mutating the Φ-clamp. (It was clearly not caused by a steric effect, as the comparably sized $-N(CH_3)_3^+$ attached at the same locations did not hinder LF_N translocation.) We have now found that the $(PA_{63}E302S/E308S/D315S)_7$ channel, despite its being less cation selective than the $(PA_{63}F427A)_7$ channel (Fig. 5 B), did not allow for the passage of LF_N once an SO_3^- group was attached (Fig. 6). Thus, it would appear once again that local electrostatic forces must be considered, and not simply macroscopic cation selectivity.

Comparison of voltage- and pH-driven translocation

As mentioned earlier, because of significant voltage-dependent gating observed in several of our asp/glu mutant channels, we were unable to perform voltage-driven translocation experiments. However, we think it is useful to briefly consider here voltage-driven translocation compared with pH-driven translocation.

In both cases, reducing the cation selectivity of the channel, and thereby allowing nonprotonated aspartates and glutamates to enter the stem, should reduce the rate of translocation of LF_N, but by different mechanisms. In the case of voltage-driven translocation, the force on the translocated peptide is reduced because its net positive charge is reduced. In the case of pH-driven translocation, the force is reduced because not all of the aspartates and glutamates "feel" the ΔpH, as they retain the same ionized state at both their entry to the channel at the cis end and their exit from the channel at the trans end.

Consider, in fact, three limiting scenarios, specifically in regard to the mechanism of protonation/deprotonation of negatively charged residues on LF_N that was discussed in this paper. In the first extreme scenario, if there were only positively charged and neutral residues on a peptide chain, translocation could be driven only by a ΔV, as pH-driven translocation requires that a Brownian ratchet be established through the protonation states of negatively charged residues. In the opposite scenario, if there were only negatively charged and neutral residues present on a peptide chain, translocation could occur only by establishing a pH gradient, as an applied positive voltage will cause translocation to occur only if the peptide has a net positive charge. Finally, in the third limiting scenario, if there were only neutral residues present on a peptide chain, then neither a ΔV nor a ΔpH would cause translocation to occur.

We thank Karen Jakes, Paul Kienker, and Russell Thomson for their assistance in performing the experiments described in this paper. We also thank Myles Akabas, Karen Jakes, and Paul Kienker for their helpful comments on the manuscript.

This work was supported by National Institutes of Health research grant GM 29210.

The authors declare no competing financial interests.

Merritt C. Maduke served as editor.

Submitted: 2 March 2015
Accepted: 9 June 2015

REFERENCES

Anderson, D.S., and R.O. Blaustein. 2008. Preventing voltage-dependent gating of anthrax toxin channels using engineered disulfides. *J. Gen. Physiol.* 132:351–360. http://dx.doi.org/10.1085/jgp.200809984

Basilio, D., S.J. Juris, R.J. Collier, and A. Finkelstein. 2009. Evidence for a proton–protein symport mechanism in the anthrax toxin channel. *J. Gen. Physiol.* 133:307–314. http://dx.doi.org/10.1085/jgp.200810170

Benson, E.L., P.D. Huynh, A. Finkelstein, and R.J. Collier. 1998. Identification of residues lining the anthrax protective antigen channel. *Biochemistry.* 37:3941–3948. http://dx.doi.org/10.1021/bi972657b

Blaustein, R.O., and A. Finkelstein. 1990. Voltage-dependent block of anthrax toxin channels in planar phospholipid bilayer membranes by symmetric tetraalkylammonium ions. Effects on macroscopic conductance. *J. Gen. Physiol.* 96:905–919. http://dx.doi.org/10.1085/jgp.96.5.905

Blaustein, R.O., T.M. Koehler, R.J. Collier, and A. Finkelstein. 1989. Anthrax toxin: channel-forming activity of protective antigen in planar phospholipid bilayers. *Proc. Natl. Acad. Sci. USA.* 86:2209–2213. http://dx.doi.org/10.1073/pnas.86.7.2209

Duesbery, N.S., C.P. Webb, S.H. Leppla, V.M. Gordon, K.R. Klimpel, T.D. Copeland, N.G. Ahn, M.K. Oskarsson, K. Fukasawa, K.D. Paull, and G.F. Vande Woude. 1998. Proteolytic inactivation of MAP-kinase-kinase by anthrax lethal factor. *Science.* 280:734–737. http://dx.doi.org/10.1126/science.280.5364.734

Finkelstein, A. 2009. Proton-coupled protein transport through the anthrax toxin channel. *Philos. Trans. R. Soc. Lond. B Biol. Sci.* 364:209–215. http://dx.doi.org/10.1098/rstb.2008.0126

Gogol, E.P., N. Akkaladevi, L. Szerszen, S. Mukherjee, L. Chollet-Hinton, H. Katayama, B.L. Pentelute, R.J. Collier, and M.T. Fisher. 2013. Three dimensional structure of the anthrax toxin translocon-lethal factor complex by cryo-electron microscopy. *Protein Sci.* 22:586–594. http://dx.doi.org/10.1002/pro.2241

Hodgkin, A.L., and B. Katz. 1949. The effect of sodium ions on the electrical activity of giant axon of the squid. *J. Physiol.* 108:37–77. http://dx.doi.org/10.1113/jphysiol.1949.sp004310

Jiang, J., B.L. Pentelute, R.J. Collier, and Z.H. Zhou. 2015. Atomic structure of anthrax protective antigen pore elucidates toxin translocation. *Nature.* 521:545–549. http://dx.doi.org/10.1038/nature14247

Katayama, H., B.E. Janowiak, M. Brzozowski, J. Juryck, S. Falke, E.P. Gogol, R.J. Collier, and M.T. Fisher. 2008. GroEL as a molecular scaffold for structural analysis of the anthrax toxin pore. *Nat. Struct. Mol. Biol.* 15:754–760. http://dx.doi.org/10.1038/nsmb.1442

Kintzer, A.F., K.L. Thoren, H.J. Sterling, K.C. Dong, G.K. Feld, I.I. Tang, T.T. Zhang, E.R. Williams, J.M. Berger, and B.A. Krantz. 2009. The protective antigen component of anthrax toxin forms functional octameric complexes. *J. Mol. Biol.* 392:614–629. http://dx.doi.org/10.1016/j.jmb.2009.07.037

Krantz, B.A., R.A. Melnyk, S. Zhang, S.J. Juris, D.B. Lacy, Z. Wu, A. Finkelstein, and R.J. Collier. 2005. A phenylalanine clamp catalyzes protein translocation through the anthrax toxin pore. *Science.* 309:777–781. http://dx.doi.org/10.1126/science.1113380

Krantz, B.A., A. Finkelstein, and R.J. Collier. 2006. Protein translocation through the anthrax toxin transmembrane pore is driven by a proton gradient. *J. Mol. Biol.* 355:968–979. http://dx.doi.org/10.1016/j.jmb.2005.11.030

Leppla, S.H. 1982. Anthrax toxin edema factor: a bacterial adenylate cyclase that increases cyclic AMP concentrations of eukaryotic cells. *Proc. Natl. Acad. Sci. USA.* 79:3162–3166. http://dx.doi.org/10.1073/pnas.79.10.3162

Mueller, P., D.O. Rudin, H. Ti Tien, and W.C. Wescott. 1963. Methods for the formation of single bimolecular lipid membranes in aqueous solution. *J. Phys. Chem.* 67:534–535. http://dx.doi.org/10.1021/j100796a529

Nassi, S., R.J. Collier, and A. Finkelstein. 2002. PA_{63} channel of anthrax toxin: An extended β-barrel. *Biochemistry.* 41:1445–1450. http://dx.doi.org/10.1021/bi0119518

Nguyen, T.L. 2004. Three-dimensional model of the pore form of anthrax protective antigen. Structure and biological implications. *J. Biomol. Struct. Dyn.* 22:253–265. http://dx.doi.org/10.1080/07391102.2004.10531226

Robinson, R.A., and R.H. Stokes. 1965. Electrolyte Solutions. Butterworths, London. 571 pp.

Schiffmiller, A., and A. Finkelstein. 2015. Ion conductance of the stem of the anthrax toxin channel during lethal factor translocation. *J. Mol. Biol.* 427:1211–1223. http://dx.doi.org/10.1016/j.jmb.2014.06.016

Teorell, T. 1953. Transport processes and electrical phenomena in ionic membranes. *Prog. Biophys. Biophys. Chem.* 3:305–369.

Vitale, G., R. Pellizzari, C. Recchi, G. Napolitani, M. Mock, and C. Montecucco. 1998. Anthrax lethal factor cleaves the N-terminus of MAPKKs and induces tyrosine/threonine phosphorylation of MAPKs in cultured macrophages. *Biochem. Biophys. Res. Commun.* 248:706–711. http://dx.doi.org/10.1006/bbrc.1998.9040

Wynia-Smith, S.L., M.J. Brown, G. Chirichella, G. Kemalyan, and B.A. Krantz. 2012. Electrostatic ratchet in the protective antigen channel promotes anthrax toxin translocation. *J. Biol. Chem.* 287:43753–43764. http://dx.doi.org/10.1074/jbc.M112.419598

Young, J.A., and R.J. Collier. 2007. Anthrax toxin: Receptor binding, internalization, pore formation, and translocation. *Annu. Rev. Biochem.* 76:243–265. http://dx.doi.org/10.1146/annurev.biochem.75.103004.142728

Zhang, S., A. Finkelstein, and R.J. Collier. 2004a. Evidence that translocation of anthrax toxin's lethal factor is initiated by entry of its N terminus into the protective antigen channel. *Proc. Natl. Acad. Sci. USA.* 101:16756–16761. http://dx.doi.org/10.1073/pnas.0405754101

Zhang, S., E. Udho, Z. Wu, R.J. Collier, and A. Finkelstein. 2004b. Protein translocation through anthrax toxin channels formed in planar lipid bilayers. *Biophys. J.* 87:3842–3849. http://dx.doi.org/10.1529/biophysj.104.050864